PET/MR: Functional and Molecular Imaging of Neurological Diseases and Neurosciences

Jie Lu
Guoguang Zhao

科学技术文献出版社
SCIENTIFIC AND TECHNICAL DOCUMENTATION PRESS

Springer

PET/MR: Functional and Molecular Imaging of Neurological Diseases and Neurosciences

Jie Lu • Guoguang Zhao
Editors

PET/MR: Functional and Molecular Imaging of Neurological Diseases and Neurosciences

科学技术文献出版社
SCIENTIFIC AND TECHNICAL DOCUMENTATION PRESS

Springer

Editors
Jie Lu
Department of Radiology
and Nuclear Medicine
Xuanwu Hospital
Capital Medical Uniersity
Beijing, China

Guoguang Zhao
Department of Neurosurgery
Xuanwu Hospital
Capital Medical University
Beijing, China

ISBN 978-981-19-9901-7 ISBN 978-981-19-9902-4 (eBook)
https://doi.org/10.1007/978-981-19-9902-4
Jointly published with Scientific and Technical Documentation Press

This Springer imprint is published by the registered company Springer Nature Singapore Pte Ltd.
The registered company address is: 152 Beach Road, #21-01/04 Gateway East, Singapore 189721, Singapore

Preface

Brain disorders seriously endanger the life and health of people in China due to their high morbidity, mortality, and disability rate. Nowadays, research, development, and clinical application of neuroimaging techniques are developing rapidly, aimed at further improving the accuracy of diagnosis of brain disorders. The invention and application of integrated positron emission tomography/magnetic resonance (PET/MR), a product of organic combination of functional brain imaging and molecular imaging techniques, is aimed at fulfilling the exploration of brain disorders and brain science. Based on the theory of brain function and molecular biology and with the help of modern medical imaging techniques, it truly realizes in vivo visualization of different parts of the signaling pathways in the human body.

Basic studies in molecular biology can fully exert their research significance only if they are applied to humans. Integrated PET/MR builds a bridge between basic research in molecular biology and its in vivo clinical application in humans. It can dynamically, objectively, and quantitatively transform the neurotransmitters, immune proteins, and tissue-specific biomarkers into intuitive spatial distribution images, followed by fusing with structural images to achieve accurate identification and delineation of lesions with high sensitivity and specificity. Moreover, integrated PET/MR can be useful to adequately identify the pathological tissues and healthy tissues, locate targets, and outline the boundaries. Using integrated PET/MR in combination with advanced innovative techniques (e.g., analysis methods for brain science, neuromodulation, surgical robots, and image-guided precision neurosurgery) can lead to new ideas for the diagnosis and treatment of neurological diseases such as glioma, brain metastases, epilepsy, and Alzheimer's disease.

This book comprehensively summarizes the latest progress regarding the application of integrated PET/MR in the diagnosis, treatment, and research of brain disorders at Xuanwu Hospital, Capital Medical University. It also introduces the latest achievements in the field of brain science in China and abroad. Each chapter offers perspective and practicability, which will help medical imaging technologists master the essentials of integrated PET/MR diagnosis. The book also has important reference value for scientific research in brain functional and molecular imaging. Therefore, it is especially suitable for practitioners in the fields of neuroimaging, neurology, neurosurgery, and other related major fields of brain science. We believe that the publication of

this book will play a vital role in promoting PET/MR in terms of basic research and clinical application.

Those who share the same desire succeed, and those who help each other win! Let us look forward to great achievements of the application of "Integrated PET/MR Brain Functional and Molecular Imaging" in brain disorders and brain science. With PET/MR and related techniques, research ranging from brain disorders to brain science is bound to make great progress!

Beijing, China Guoguang Zhao

Preface

Time flies, and 7 years have passed in the blink of an eye. Looking back on the installation and use of positron emission tomography/magnetic resonance (PET/MR) equipment 7 years ago (July 2015), it seems like only yesterday. I can still vividly remember the feeling when I welcomed the first time-of-flight PET/MR equipment in Southeast Asia. I had no experience and no team at that time, but I confronted the challenge with complete enthusiasm, and concomitantly bore the huge psychological pressure of fearing failure and living up to the expectations of the leaders of our hospital. Relying on my skills in magnetic resonance imaging (MRI), I led a novice team consisting of a newly enrolled graduate student (Bixiao Cui) with a background in nuclear medicine, a nuclear medicine technologist (Jie Ma) with only 2 months of experience in PET/CT, and a nurse (Dongmei Shuai) to start the exploration in PET/MR. The hardships are indescribable. The efforts of countless all-nighters, weekends, and holidays gradually paid off, resulting in my first speech in an international conference, publication of our first PET/MR monograph, and publication of our first article in European Journal of Nuclear Medicine and Molecular Imaging! These 7 years were full of sweat, tears, toil, and pain, as well as the joy of harvest and success! Over the past 7 years, the team has also continued to grow and expand, forming an integrated cross-functional team of members specializing in medicine and engineering, and research groups specializing in various brain disorders including cerebrovascular disease, brain tumor, epilepsy, Alzheimer's disease, and Parkinson's disease. Every member has injected new vitality into the team and contributed to new results. At this point, I would like to thank them sincerely for their hard work, dedication, and persistence and for their company throughout this journey, which has given me the courage to keep going forward.

With the development of PET/MR equipment and its popularization and application in our country, there is an urgent need for interdisciplinary talents who are skilled in PET and MRI in clinical practice. Our previous publications including *Integrated PET/MR: Operation Specifications and Clinical Application*, *Integrated PET/MR Practice Manual*, and *Integrated PET/MR Imaging: Case Atlas* mainly focused on the standardization of clinical operation of the equipment and manifestations of typical clinical cases. Based on previous work, this book summarizes our team's experience in studying brain disorders and brain science as well as the latest research progress in China and abroad. It comprehensively introduces the research progress in PET/MR brain functional and molecular imaging including its clinical application in

brain disorders and the status quo of brain science. The book consists of 16 chapters including introduction of the equipment, principles of functional brain imaging, its application in brain disorders, and research in brain science, gradually deepening chapter by chapter. The content related to functional brain imaging includes functional MRI, perfusion imaging, principles of dynamic PET imaging, and data post-processing methods. The related brain disorders include Alzheimer's disease, Parkinson's disease, epilepsy, brain tumor, cerebrovascular disease, brain injury, depression, schizophrenia, multiple sclerosis, migraine, and other major diseases. Therefore, this book has great clinical practicability.

We have received great support and help from many colleagues while writing this book. We would like to express our deep gratitude to Professor Jiehui Jiang from Shanghai University; Professor Lijun Bai from Xi'an Jiaotong University; Professor Su Lui from West China Hospital of Sichuan University; Professor Jiliang Fang from Guang'anmen Hospital, China Academy of Chinese Medical Sciences; Professor Baoci Shan from the Institute of High Energy Physics, Chinese Academy of Sciences; Professor Chuantao Zuo from Huashan Hospital of Fudan University; Professor Yufeng Zang from Hangzhou Normal University; Professor Xiang Li from Vienna General Hospital, Medical University of Vienna; Professor Jun Liu from the Second Xiangya Hospital of Central South University; Professor Yong He from Beijing Normal University; and Professor Junling Xu from Henan Provincial People's Hospital. They participated in the writing of this book in their spare time and provided valuable opinions and suggestions despite their busy work schedules. I would like to express my heartfelt thanks to them! Due to the limited knowledge of the author, inadequacies and omissions are inevitable in the book, and all colleagues are welcome to offer criticism and corrections.

Beijing, China Jie Lu

Contents

About the Editors

Guoguang Zhao, M.D., Ph.D. Prof. Zhao is the President of Xuanwu Hospital, Capital Medical University, National Medical Center for Neurological Disorders, the coordinator of the China International Neurosurgery Institute and the director of the national neurosurgical robot committee. Prof. Zhao has focused on stereotactic neurosurgery and brain functional diseases. He has dedicated himself to the promotion and application of neurosurgical robots in China, where he co-developed China's first neurosurgical robot. To date, Prof. Zhao has published over 50 papers in prestigious journals such as *The Lancet Public Health, Alzheimer's & Dementia, and Science Bulletin*, of which the highest impact factor was 72. Prof. Zhao has presided over projects of the National Key Research & Development Program, and National Natural Science Foundation, and edited or translated five books.

Jie Lu, M.D., Ph.D. Prof. Lu is the Vice President and the Director of Department of Radiology and Nuclear Medicine, Xuanwu Hospital, Capital Medical University, mainly engaged in brain function and molecular imaging research. Her team took the lead in the multi-modal imaging research of brain diseases using PET/MR, developing new individualized technology and innovative scanning sequence for brain function analysis. To break through the difficult problem of individualized application, Prof. Lu independently developed deep learning technology for the diagnosis of brain disease by multi-modal neuroimaging methods and established a full-process automatic platform for image post-processing and diagnosis. To date Prof. Lu has published more than 200 SCI articles as the first or corresponding author, with the representative works published in international authoritative journals such as *Neuron, Nat Commun, Radiology, Brain, Neurology, EJNMMI*. Among them, the most cited article was cited for 495 times, listed in the top 1% ESI highly cited papers. Prof. Lu was the main editor of 6 PET/MR monographs, authorized 7 related patents, chaired or participated in 12 expert consensuses, presided over 18 research projects. Prof. Lu now serves as the editorial board of several international academic journals, such as EJNMMI, Neuroimage, and JMRI.

1 Introduction to Positron Emission Tomography/Magnetic Resonance (PET/MR) Imaging

Bixiao Cui, Kun Guo, and Jie Lu

Molecular imaging is an emerging interdisciplinary field that integrates multiple disciplines including medical imaging, nuclear medicine, clinical medicine, molecular biology, chemistry, physics, and computer science. Molecular imaging can be used to observe molecular and biological functions in the living body. Positron emission tomography/magnetic resonance imaging (PET/MR) combines PET and MRI into a single modality and is currently the most advanced medical imaging available.

1.1 History of PET/MR

During the past few decades, there has been growing interest in multimodal imaging equipment. A large number of studies have shown that the combination of two or more imaging modalities can improve diagnostic performance. Thus, in 1998, the first PET/computed tomography (PET/CT) system was created, which was widely accepted by medical imaging experts, clinicians, and molecular imaging researchers worldwide. PET/CT integrates both PET and CT into a single machine, providing a multimodal imaging approach that has now become a routine diagnostic tool in clinical practice. However, the clinical application of PET/CT has several shortcomings. First, although the information acquired using CT can assist physicians in determining the anatomical location of lesions, it has a lower image resolution for soft tissues than that obtained using MRI. Second, MRI does not emit ionizing radiation, and therefore, it is more suitable for children as well as patients who may need to undergo repeated examinations. PET is a type of functional imaging technique that can detect abnormalities in the metabolism of various human tissues with extremely high sensitivity and accuracy. Therefore, the integration of PET and MRI into a single system enables the acquisition of a full range of data regarding the structure, function, and metabolism of the human body. This information is highly valuable in the diagnosis and treatment of diseases. Due to the complementary characteristics of MRI and PET, researchers began exploring the potential of integrated PET/MR systems.

In 1990, the first structural design patent was issued for inclusion of a PET detector in an MRI scanner. In 1997, researchers placed scintillation crystals within a 0.2 Tesla (T) open MRI system and connected them to photomultiplier tubes (PMTs) housed outside of the magnetic field via 4 m long optical fibers; they used this technology to perform PET/MR on anatomical phantoms. However, progress of the early development of the integrated PET/MR technology was slow due to compatibility-related difficulties, such as the

B. Cui · K. Guo · J. Lu (✉)
Department of Radiology and Nuclear Medicine, Xuanwu Hospital, Capital Medical University, Beijing, China

J. Lu, G. Zhao (eds.), *PET/MR: Functional and Molecular Imaging of Neurological Diseases and Neurosciences*, https://doi.org/10.1007/978-981-19-9902-4_1

feasibility of placing PET detectors within the magnetic field of the MRI scanner and PET image attenuation correction.

To minimize the mutual interference between PET and MRI technologies, one of the key technical requirements was the development of PET detectors and photodiodes that could detect 511 KeV high-energy photons in a strong magnetic field. Previous studies found that the scintillation crystals used in PET/MR needed an electromagnetic compatibility close to that of the human body to be effective. However, the electromagnetic compatibility of traditional scintillation crystals, such as lutetium gadolinium oxyorthosilicate and gadolinium oxyorthosilicate, differs significantly from that of the human body. This difference can affect the homogeneity of the magnetic field of the MRI scanner, producing artifacts that preclude the use of these materials in PET/MR. However, the increased research activity and clinical use of cerium-doped lutetium oxyorthosilicate (LSO) and cerium-doped lutetium yttrium oxyorthosilicate (LYSO) effectively solved the problem of electromagnetic susceptibility. Additionally, the PMTs traditionally used in PET/CT systems were highly susceptible to magnetic fields; however, the magnetic field of the MRI system can alter the trajectory and skew the detection of electrons, indicating that PMTs are not feasible in PET/MR systems.

Avalanche photodiodes (APDs), however, are not affected by magnetic fields and can be coupled with PET scintillation crystals directly or via very short optical fibers. Studies evaluating APD-based PET/MR have been conducted in both small animals and the human brain. Furthermore, ADP-based PET/MR for whole-body imaging has been successfully developed and utilized; the Biograph mMR by Siemens combines LSO crystals and APDs to enable both the detection of gamma (γ) particles in strong magnetic fields and the conversion of scintillation photon signals to electrical signals. However, despite the relative maturity of the APD technology, APDs are limited by their low signal amplification gain (10^2–10^3), slow output signal, and low temporal resolution. In recent years, improved detectors using silicon photoelectric multipliers (SiPMs) have gradually become a technological hotspot in PET/MR research. SiPMs have the same amplification gain and temporal resolution as traditional PMTs, as well as other advantages such as improved consistency, small size, low operating voltage, and compact structure. Xi et al. used SiPMs to construct a monolithic PET detector array and calculated the optimal size of the SiPM array for clinical imaging, which yielded a relatively high detection efficiency. SiPMs are sensitive to temperature, implying that the stability of the signal output depends on the bias voltage and temperature changes. With the continuing advances in temperature control technology, it will soon be possible to resolve the issue of temperature sensitivity in SiPMs.

Rapid progress has been made in the development of integrated PET/MR technology, due to the increasing sophistication of new photoelectric detection technology. In November 2006, the Knoxville Medical Center in Knoxville, Tennessee, USA, used an integrated Siemens PET/MR scanner to perform the world's first simultaneous acquisition of human brain fusion images. In 2011, Phillips unveiled the 3.0T sequential Ingenuity TF PET/MR scanner (Fig. 1.1a), which combined MRI with a redesigned PET component with special magnetic shielding. In the same year, Siemens released the integrated Biograph mMR PET/MR scanner (Fig. 1.1b), which allowed for the fused acquisition of MR and PET images within the same machine, enabling synchronous and concentric MR and PET imaging. At the end of 2014, General Electric launched the world's first integrated PET/MR scanner with time of flight (TOF) function (Fig. 1.1c). The introduction of TOF technology significantly shortened the scan time, reduced the dose of radiopharmaceuticals administered to patients, and significantly enhanced the image contrast. In the same year, Siemens released the second-generation integrated Biograph mMR PET/MR scanner, which was equipped with high-definition PET technology (HD PET) that improved the resolution, contrast, and signal-to-noise ratio of PET images. In addition, the application of its unique BodyCOMPASS

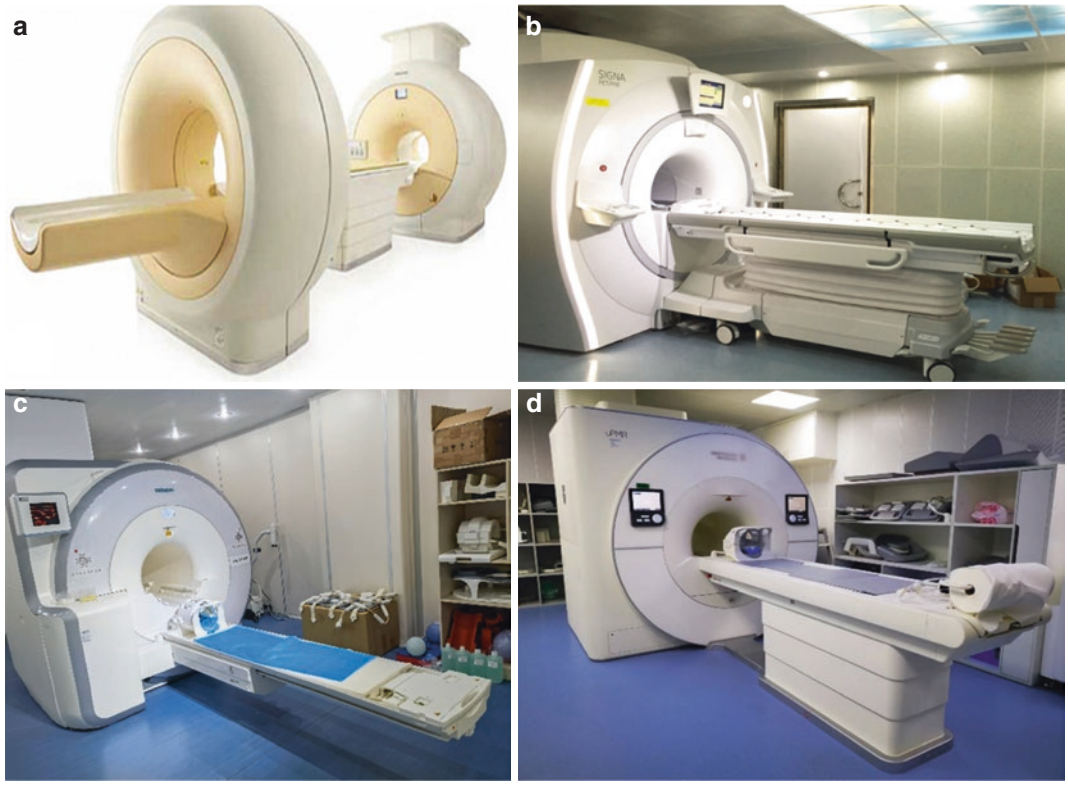

Fig. 1.1 PET/MR scanners: sequential Ingenuity TF PET/MR (**a**); integrated Biograph mMR PET/MR (**b**); integrated Signa TOF PET/MR (**c**); and integrated uPMR 790 PET/MR (**d**)

technology enabled MRI-based PET calibration during functional imaging, so as to ensure data accuracy. In China, research on PET/MR began relatively late compared to other countries. In 2018, United Imaging launched the uPMR 790 PET/MR scanner (Fig. 1.1d), which was fully integrated with artificial intelligence technology. Deep learning methods were implemented to achieve a series of unique innovations in imaging workflow automation, including one-click intelligent localization, bed planning, and attenuation correction, simplifying the workflow while also enhancing the quality of standardized imaging.

1.2 PET/MR Equipment

The integrated PET/MR scanner is a novel multimodal imaging system that merges PET and MRI into a single machine. This configuration enables two different simultaneous acquisition of data by two different modalities within the same space, while also drawing on the independent functions of each equipment. Therefore, PET/MR combines high soft tissue resolution and multiparameter, multi-functional imaging characteristics of MRI, with high sensitivity for radiotracer metabolism and quantitative characteristics of PET into a single system.

1.2.1 Components of the Integrated PET/MR System

The hardware of the integrated PET/MR system is primarily composed of a gantry, examination table, and console. Other components include the corresponding coils, cabinets, and post-processing workstation. The gantry consists of the PET and MRI components, and its basic structure (from inner- to outermost) includes the MRI body coil, PET detector module, MRI

gradient coil, main magnetic field coil, and magnetic field shielding coil. The PET detector module of the integrated PET/MR system is composed of the photoconductive radiofrequency (RF) shielding module, lutetium-based scintillators (LBSs), SiPMs, thermal coupling gasket, and aluminum fixation gasket. The photoconductive RF shielding module eliminates electromagnetic interference from the MRI components, whereas the LBSs intercept photons; the SiPMs convert photon signals into electrical signals, and the thermal coupling gasket conducts heat and maintains the detector at a constant temperature. The aluminum fixation gasket fixes the detector module in place. The primary coils of the integrated PET/MR system include the joint head/neck coil, body coil, breast coil, and flexible coils (Fig. 1.2).

The console is composed of a display and keyboard, which includes control buttons for initiating scanning on the display, adjusting the examination table, and communicating with the patient. The equipment cabinet room houses a variety of equipment, including the MRI RF cabinet, PET cabinet, conduction plate cabinet, heat exchanger cabinet, PET water cooling system, helium compressor, and magnet monitor. The MRI RF cabinet provides the system's RF gradient and generates and controls equipment signals. The PET cabinet houses the PET power supply unit and PET reconstruction computer. The conduction plate cabinet contains other auxiliary power supplies. The heat exchanger cabinet is used for the system's air and water cooling, as the PET detector is cooled by the PET water cooling system. The helium compressor controls the magnetic pressure using helium gas, while the magnet monitor allows for observation of the magnetic pressure and liquid helium level. The image post-processing system processes image data transmitted to the post-processing workstation, which requires hardware with a high storage capacity, large memory, and fast computing power, together with supporting post-processing software, and typically uses miniaturized high-performance computers.

Fig. 1.2 MRI surface coils: joint head/neck coil (**a**); body coil (**b**); breast coil (**c**); and flexible coil (**d**)

1.2.2 Hardware Compatibility

Integrated PET/MR involves integration of a full-ring PET detector into the gradient and RF transmitter coils of the MRI system. While the RF and gradient coils emit RF and gradient pulses, the PET detector receives the γ photons released after positron emission decay, thereby achieving fully iso-field and iso-centric imaging. As the PET detector is embedded in the MRI system, substantial improvements to the RF transmitter and gradient coils are needed. Therefore, the device thickness had to be decreased, to make room for installation of the PET detector while maintaining adequate MRI performance; moreover, the bore diameter is often reduced to 60 cm.

The core challenge in successful deployment of an integrated PET/MR system lies in ensuring compatibility of the PET and MRI hardware. Therefore, the scintillation crystals used for PET imaging must have low magnetic susceptibility. However, traditional scintillation crystals, such as lutetium gadolinium oxyorthosilicate and gadolinium oxyorthosilicate, are highly susceptible to a magnetic field, which can affect the homogeneity of the magnetic field of MRI components, easily creating artifacts. SiPM-based Geiger-mode detectors are small in size, with low operating voltage, a compact structure, and decreased susceptibility to magnetic fields. They have superior energy resolution and temporal resolution when compared to APDs. Therefore, they are the preferred choice for photoelectric conversion detectors in integrated PET/MR systems.

1.2.3 Principles of PET/MR Imaging

1.2.3.1 Principles of PET Imaging

In PET imaging, a molecular substance required for metabolism in the body is labelled with a positron-emitting radionuclide, which releases positrons as it decays. The positrons then interact with free electrons in the body to generate annihilation radiation, emitting two γ photons with the same energy (511 keV) in opposite directions. The PET scanner detects the pair of γ photons within a specific time frame (i.e., the coincidence time window) to confirm the occurrence of an annihilation event between the two detectors, and the event is recorded as one event. Since γ photons have a certain level of penetrating power, PET detects γ photons outside of the body to obtain the tomographic distribution of positron-emitting radionuclides for imaging. The PET detector is ring-shaped, and volume data are obtained by detecting the resulting γ photon pairs from annihilation events in any direction within the detector.

1.2.3.2 Principles of MR Imaging

In MRI, the most commonly used atomic nucleus is the hydrogen proton because of its high magnetic susceptibility and wide distribution in human tissues. Each hydrogen proton within the body acts as a miniscule magnet; however, the chaotic arrangement of protons throughout the body causes their magnetization vectors to negate each other and therefore fail to produce a macroscopic magnetization vector. Upon entering the main magnetic field, however, the magnetic field generated by the spin of protons becomes parallel with the main magnetic field, rotating and swinging around the axis of the main magnetic field—a type of rotation known as precession. When an RF pulse that matches the precession frequency of protons is used to excite the nuclei, the energy of the RF pulse is transferred to the protons at a low level, exciting them to a higher energy level; this phenomenon is known as magnetic resonance. The energy of the RF pulse deflects the macroscopic magnetization vector, which gradually returns to a state of equilibrium when the RF pulse is turned off. The time it takes to return to a state of equilibrium is known as relaxation time. Relaxation is divided into two parts: (1) longitudinal relaxation, which is the gradual return of the longitudinal magnetization vector to its initial maximum value (equilibrium state), while T1 relaxation is the time needed to return to 63% of its initial maximum value; and (2) transverse relaxation, which is a gradual decrease of the transverse magnetization vector until it disappears, while T2 relaxation is the time needed for it to decay to 37% of its maximum value. The number of protons varies between different

tissues in the human body, resulting in different T1 and T2 values. To highlight one tissue characteristic, weighted imaging techniques can be utilized to suppress the other characteristics as much as possible.

1.2.3.3 Attenuation Correction Technology

The 511 keV high-energy photons detected during PET cause the Compton effect to occur in the human body, during which high-energy protons are either attenuated or scattered. Attenuation correction algorithms are used to estimate the attenuation and scattering ratio of each line of response. The resultant images only provide information on proton density and relaxation time and do not provide an attenuation profile. MR-based attenuation correction (MRAC) is achieved using tissue segmentation, atlas registration, transmission scan, and emission data reconstruction methods.

The most recent integrated TOF PET/MR scanners can perform sensitivity, radionuclide attenuation, and detector dead time corrections on the PET detector, similar to the capabilities of traditional PET and PET/CT. However, γ-ray attenuation, γ-ray random coincidence, and γ-ray scatter corrections are all based on information obtained during MRI. Due to the limited field of view in MRI, it is necessary to combine the MRI signals with the TOF information from PET with no attenuation correction (NAC) in order to restore the contours of the human body. First, the MRI sequence is used to acquire information on water, gas, soft tissue, adipose tissue, and/or bone in the human body, which is combined with PET-NAC to restore the contours of the body. Next, the MRAC attenuation correction map (MRAC μ-map) is obtained for application to the PET images. Adipose tissues have a relatively small attenuation coefficient, but they exhibit high signal intensities in both T1- and T2-weighted MR images; therefore, information on adipose tissue can be isolated in the process of tissue segmentation. To improve accuracy, the matrix of the MRAC μ-map is similar in size to that of the PET scan. Given the structural complexity of human tissues, the use of human body atlases can enhance the speed and accuracy of tissue segmentation. Furthermore, MRI with zero echo time (ZTE) is crucial for accurate depiction of bone structure. As the density of bone cortex is almost three times the average density of bone, precise MRAC can only be achieved using the cortical bone structure. Traditional methods employ ultrashort echo time (UTE) to acquire the overall bone structure, but this technique is insufficient to obtain the cortical bone structure. ZTE, however, can accurately obtain the anatomical structure of the cortical bone. Additionally, TOF technology can help eliminate the impact of foreign bodies on MRAC, thus improving the accuracy of the resulting PET images.

1.3 PET/MR Scan Protocols

Integrated PET/MR involves simultaneous acquisition of PET and MRI. Prior to scanning, the PET parameters are defined before setting the MRI sequences. The main scan modes in integrated PET/MR include a PET scan and an MRI scan. In accordance with actual clinical needs, simultaneous PET and MRI scanning can first be performed, followed by separate scans with certain special MRI sequences (e.g., contrast-enhanced MRI). This section will mainly introduce PET/MR scans of the brain.

1.3.1 Pre-Scan Preparation

Patients must fast for at least 4 h before the scan, although they can drink sugar-free water during this period, and they must also avoid exercising vigorously or for an extended period of time the day prior to the scan. Diabetic patients should maintain their blood glucose concentration at a recommended level of ≤11.1 mmol/L. Patients should disclose their current medication regimens and be accompanied by a family member on the day of the scan. The attending physician obtains a detailed medical history, verifies the patient's order, and confirms the patient's general

information, reason for the examination, and scan protocol. The physician also verifies that the patient has no contraindications to MRI, and informs the patient of the scan procedure, precautions, and expectations.

On the day of scan, the patient's height, weight, and blood glucose are measured, and venous access is established. The injection dose is calculated based on body weight, which is 3.7 MBq/kg for the conventional tracer ^{18}F-fluorodeoxyglucose (^{18}F-FDG), and 0.1 mL/kg body weight (0.1 mmol/kg) for the contrast agent. For patients undergoing static imaging, all audiovisual stimuli are blocked out after the radioactive tracer (e.g., ^{18}F-FDG) is injected, the room lights are dimmed, and the temperature is maintained at approximately 22 °C. The patient is asked to keep their eyes closed for 40–60 min while lying on the examination table, during which they should avoid talking, eating, or chewing. For patients undergoing dynamic imaging, a bolus injection of the radioactive tracer is performed with the patient on the scan table, and the technologist begins image acquisition before the injection. Patients receiving dual radioactive tracers are first injected with the tracer with the shortest half-life. They are scanned, and then asked to rest on the scan table with their eyes closed for ≥10 half-lives, after which they are injected with the tracer with a longer half-life. Patients receiving both a radioactive tracer and a contrast agent are injected via two separate intravenous (IV) catheters, so as to prevent the accumulation of radioactive tracers in the IV catheter from affecting image quality. Patients are required to change into hospital provided clothes for the examination; prior to entering the scan room, the patient and their family member/friend must remove all metallic objects from their bodies. Wheelchairs, stretchers, hospital beds, oxygen tanks, monitoring equipment, and other equipment are all strictly prohibited from entering the examination room. Patients requiring oxygen therapy are given MRI-safe oxygen equipment. Patients with limited mobility should use MRI-safe wheelchairs or beds. Nurses are strictly prohibited from bringing any metallic items into the scan room.

1.3.2 PET/MR Data Acquisition

1.3.2.1 Scanning Coils and Body Positions for Integrated PET/ MR

During integrated PET/MR, the joint head/neck coil is used, and the patient wears earplugs to protect their hearing. The patient is placed in the supine position, entering the scanner head first, with both arms by their sides. The long axis of the body should be parallel to the long axis of the scan table, and the coil should be placed close to the shoulders. The head should remain motionless and centered in the scanner, and can be positioned using a head wedge. Due to the small size of children's heads, support cushions can be used to raise the head, centering it with the coil as much as possible, while asking the patient to retract their lower mandible. The glabella or nasal base is used for centering the patient's position, and the patient must close their eyes when the laser light passes over them. The technologist should also instruct the patient to use the alert button if they experience any significant discomfort. The anatomical scan range includes the entire brain, from the foramen magnum through the top of the skull. Details on the scanning process are shown in Fig. 1.3.

1.3.2.2 PET Scan Parameters

PET imaging of the brain consists of a single scan position, and the scan range includes the entire brain. The midline of the scan position is the center of the brain. Acquisitions can either be considered static or dynamic, as previously described in Sect. 3.1. The scanning mode is set to volume scan, which covers the entire brain. The dynamic scan time begins after the injection of the radioactive tracer with the patient on the scan table, and ends when drug metabolism stabilizes, which generally takes around 60 min. The scan time can be selected based on the characteristics of the tracer used. Static scans generally last 8–10 min, or are performed simultaneously with the MRI scan. The scan parameter settings (based on the GE PET/MR) are as follows: TOF and point spread function (PSF) technology; slice

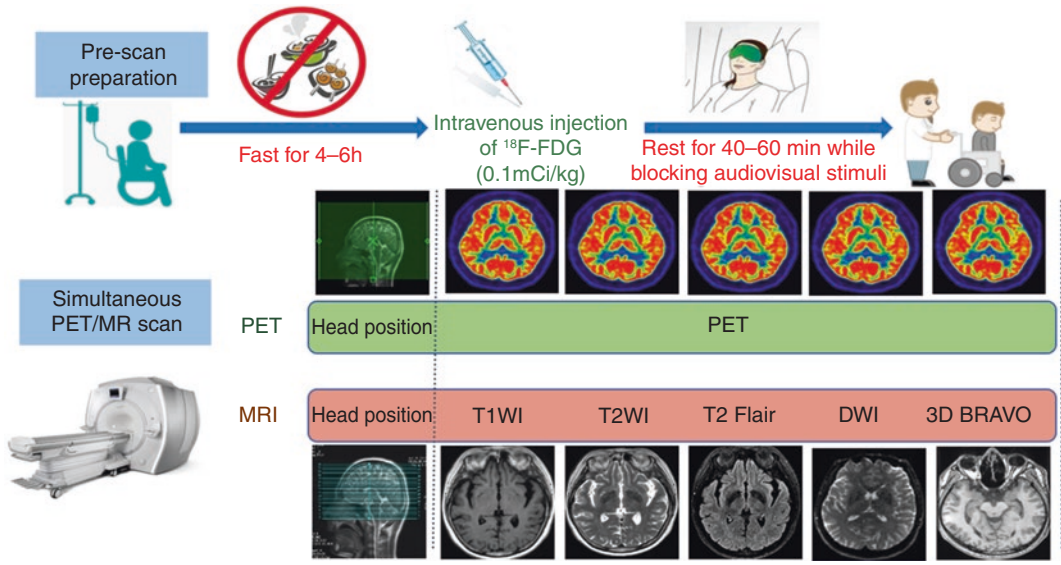

Fig. 1.3 Schematic diagram of the integrated PET/MR scanning procedure

thickness = 2.78 mm; field of view (FOV) = 35 cm; number of iterations = 8; valid subset = 32; matrix size = 192 × 192; full width at half maximum = 3 mm; and MRAC based on the Dixon sequence. The list mode is selected in dynamic scanning for segmenting in chronological order, which is necessary for image reconstruction.

1.3.2.3 MRI Scan Parameters

(1) Conventional MRI sequences: The scan range includes the entire brain, from the foramen magnum through the top of the skull. Conventional scan orientations include the transverse, sagittal, and (when necessary) coronal planes. Transverse scanning is performed parallel to the anteroposterior lines; sagittal scanning is performed parallel to the longitudinal fissure of the brain; and coronal scanning is performed with reference to the sagittal and transverse planes, perpendicular to the longitudinal fissure on the transverse plane and parallel to the brain stem on the sagittal plane. The scan range is determined based on the size of the lesion. Nonenhanced sequences obtained include transverse T2-weighted imaging (T2WI), T1-weighted imaging (T1WI), fluid-attenuated inversion recovery (FLAIR), diffusion-weighted imaging (DWI), sagittal T2WI or T1WI, and coronal T2WI or T1WI; fat-suppressed T1WI can also be performed if necessary, depending on the lesion. The scan parameters (based on the GE PET/MR) are as follows:

- T2WI: transverse scan; repetition time (TR) = 5.758 ms; echo time (TE) = 120 ms; FOV = 23 cm; matrix size = 256 × 256; number of excitations (NEX) = 1; slice thickness = 5.0 mm; interslice gap = 1.0 mm; and scan time = 1 min 9 s. The scan range covers all brain tissue from the skull base through the top of the skull.
- T1WI: transverse scan; TR = 2.529 ms; TE = 11 ms; FOV = 23 cm; matrix size = 256 × 256; NEX = 2; slice thickness = 5.0 mm; interslice gap = 1.0 mm; and scan time = 2 min 47 s. The scan range covers all brain tissue from the skull base through the top of the skull.
- FLAIR: transverse scan; TR = 7.000 ms; TE = 155 ms; FOV = 23 cm; matrix size 256 × 256; NEX = 1; slice thickness = 5.0 mm; interslice gap = 1.0 mm; and scan time = 1 min 52 s. The scan range covers all brain tissue from the skull base through the top of the skull.

- DWI: transverse scan; TR = 2.500 ms; TE = 79.9 ms; FOV = 23 cm; matrix size = 160 × 160; *b*-values = 0 and 1.000 s/mm^2; NEX = 2; slice thickness = 5.0 mm; interslice gap = 1.0 mm; and scan time = 1 min 9 s. The scan range covers all brain tissue from the skull base through the top of the skull.

(2) Special MRI sequences: The following special sequences can be utilized, depending on the lesion. Common sequences include the following:

- Three-dimensional T1-weighted imaging (3D-T1WI): sagittal scan; TR = 7.9 ms; TE = 3.2 ms; FOV = 25.6; matrix size = 256 × 256; NEX = 1; slice thickness = 1.0 mm; interslice gap = 0 mm; voxel size = 1.00 × 1.00 × 1.00 mm^3; and scan time = 3 min 48 s. The scan range covers all brain tissue from the skull base through the top of the skull.
- Three-dimensional TOF magnetic resonance angiography (MRA): transverse scan; TR = 4 ms; TE = 17.2 ms; FOV = 22 cm; matrix size = 368 × 211; NEX = 1; slice thickness = 1.2 mm; interslice gap = 0 mm; voxel size = 0.85 × 0.6 × 1.2 mm^3; and scan time = 2 min. The scan range covers all brain tissue from the skull base through the top of the skull and is centered on the circle of Willis from the top of the corpus callosum to the foramen magnum, or encompasses the target vascular region. This sequence does not have an interslice gap and involves scanning and stitching together 3–4 slices with an overlap of 20–30%. The pre-saturation band is set above the scan area (top of skull). Flow compensation, magnetization transfer, fat suppression, and slice interpolation techniques should be utilized.
- Blood-oxygen-level-dependent functional MRI (BOLD-fMRI): echo planar imaging (EPI) sequence; transverse scan; scan range covers the skull base through the top of the skull, with the topmost slice encompassing the gray matter structure of the entire brain; TR = 2.000 ms; TE = 30 ms; FOV = 22.4 cm; matrix size = 64 × 64; NEX = 1; slice thickness = 3.5 mm; interslice gap = 0.7 mm; voxel size = 3.5 × 3.5 × 3.5 mm^3; scan time = 10 min 53 s; and time points ≥ 200. BOLD-fMRI is an imaging technique that reflects the functional activity of local brain tissue through changes in deoxyhemoglobin levels of cerebral blood vessels. Since deoxyhemoglobin is a paramagnetic substance, the decrease in deoxyhemoglobin levels during local brain activity manifests as an increase in T2 signal intensity on fMRI. BOLD signals do not directly reflect the physiological state of neural activity, but are comprehensive effects of secondary physiological responses in the surrounding blood vessels, blood flow, and metabolism elicited by neural activity.
- Diffusion tensor imaging (DTI): EPI sequence; transverse scan; TR = 8461 ms; TE = 75.1 ms; FOV = 22.4 cm; matrix size = 64 × 64; NEX = 1; slice thickness = 3.5 mm; interslice gap = 0 mm; voxel size = 3.5 × 3.5 × 3.5 mm^3; scan time = 9 min 56 s; frequency encoded in left/right direction; *b*-values are generally 0 and 1000; number of diffusion gradient directions ≥ 30; and scan range covers the skull base through the top of the skull. DTI is a non-invasive structural imaging method developed based on DWI. It uses the anisotropic diffusion of water molecules in the central nervous system to obtain information on microstructural changes at the molecular level and therefore indirectly infers pathophysiological changes. DTI can be used to acquire the diffusion characteristics of tissues, and its main parameters include mean diffusivity (MD) and fractional anisotropy (FA). The FA value is the ratio of anisotropy of the diffusion process to the overall diffusion, and its value ranges between 0 and 1, with 1 indicating maximum anisotropy in diffusion motion and 0 indicating minimum

anisotropy (i.e., maximum isotropy). FA provides information on the direction of diffusion, which can indicate the cellular arrangement and structural integrity of white matter bundles in the brain. Any pathological process that alters tissue integrity and direction of nerve fiber arrangements can lead to changes in the barriers that restrict the motion of water molecules, thereby causing changes in MD and FA.

- Susceptibility- weighted imaging (SWI): transverse scan; TR = 0.8 ms; TE = 20 ms; FOV = 23 cm; matrix size = 448 × 195; NEX = 1; slice thickness = 2.0 mm; no interslice gap; voxel size = 1.03 × 0.51 × 2 mm^3; scan time = 4 min 21 s; frequency encoded in left/right direction; phase encoded in anterior/posterior direction; and reconstructed images include phase and magnitude maps. SWI primarily shows intracerebral venules, hemorrhages, and even microbleeds, and is a valuable technique for diagnosis of traumatic brain injury, brain tumors, cerebrovascular malformations, cerebrovascular diseases, and certain neurodegenerative diseases. The 3D-SWI sequence involves scanning on the oblique plane and encompasses the entire brain, with adjustments made on the sagittal plane to avoid skull base structures, thereby reducing the impact of susceptibility artifacts from the skull base.
- Arterial spin labelling perfusion-weighted imaging (ASL-PWI): This sequence must be completed before contrast-enhanced scans, as the presence of contrast makes it impossible to perform quantitative analysis of cerebral blood flow. Post-labelling delay (PLD) is selected based on cerebral blood flow velocity, where a shorter PLD (1–1.5 s) is used for a faster blood flow, and longer PLD (1.5–2.5 s) for a slower blood flow. The general parameters are as follows: transverse scan; TR = 5500 ms; TE = 13.78 ms; FOV = 22.4 cm; matrix size = 64 × 64; NEX = 1; slice thickness = 6.0 mm; interslice gap = 0.0 mm; voxel size = 3.5 × 3.5 × 6 mm^3; scan time = 3 min 44 s; and scan range is from the skull base through the top of the skull. ASL uses an inversion recovery pulse sequence to label water protons in the arterial blood at the proximal end of the imaging plane, in order to produce blood flow-dependent image contrast.
- Perfusion-weighted imaging (PWI): EPI sequence; transverse scan; frequency encoded in the left/right direction; TR = 1.600 ms; TE = 35 ms; FOV = 23 cm; matrix size = 128 × 128; NEX = 1; slice thickness = 5.0 mm; interslice gap = 1.0 mm; voxel size = 1.8 × 1.8 × 5 mm^3; total number of scans = 40–50; contrast injection speed is generally >3–3.5 mL/s; scan time = 1 min 41 s; and scan range covers the skull base through the top of the skull. Parameters include cerebral blood flow (CBF), cerebral blood volume (CBV), mean transit time (MTT), and time to peak (TTP).
- Proton magnetic resonance spectroscopy (^{1}H-MRS): This sequence is generally not performed simultaneously with PET, in order to ensure the homogeneity of the local magnetic field. The skull, gas, fat, and major blood vessels should be avoided during positioning. This sequence requires the single-voxel spectroscopy pre-scan water peak suppression rate to be >99% and full width at half maximum <7, or multi-voxel spectroscopy pre-scan water peak suppression rate >96% and full width at half maximum <10. Scan parameters are as follows: axial scan; frequency encoded in the left/right direction; TR = 1.500 ms; TE = 144 ms; FOV = 16 cm; matrix size = 14 × 14; NEX = 2; slice thickness = 15 mm; voxel size = 10 × 10 × 15 mm^3; and scan time = 4 min 28 s. MRS utilizes the chemical shifts of various substances to discern different mole-

cules and their concentrations in a variety of biological tissues. In MRS, the region of interest (ROI) must be placed at the center slice of the lesion, which means that simultaneous iso-centric scanning with PET cannot be performed. The ROI should include the lesion and the surrounding or contralateral normal brain parenchyma, in order to facilitate the comparison between diseased and normal brain tissue. To ensure homogeneity of the local magnetic field, tangential saturation bands must be added if interfering tissues (e.g., skull, gas, fat) are present around the ROI. MRS utilized nuclear magnetic resonance and chemical shifts to achieve the quantitative analysis of specific atomic nuclei and their compounds. Therefore, it is an effective technique for non-invasive *in vivo* assessment of tissue metabolism. The main metabolites detected by ^{1}H-MRS include *N*-acetylaspartate (NAA), choline (Cho), creatine/phosphocreatine (Cr), and lactate (Lac). Of these metabolites, NAA is only found in neurons and is regarded as a neural biomarker; Cho is primarily involved in the synthesis of cell membrane phospholipids and acetylcholine; Cr is an energy metabolite with relatively stable levels and is therefore often used as a reference value to standardize the levels of other metabolites; Lac is a product of anaerobic glycolysis, and an early, sensitive marker of cerebral ischemia.

(3) Special MRI sequences for different neurological diseases:
- Cerebrovascular diseases: SWI (to reveal cerebral microbleeds); PWI or ASL (to evaluate impairments in whole-brain blood perfusion); or MRA (to detect intracranial arterial diseases).
- Intracranial space-occupying lesions: contrast-enhanced 3D-T1WI (to better display brain metastases) and ^{1}H-MRS (to help differentiate between malignant and benign tumors).
- Epilepsy: oblique coronal FLAIR, angled perpendicular to the hippocampus (to show abnormal hippocampal signals).
- Alzheimer's disease: oblique coronal T1WI, angled perpendicular to the hippocampus (to detect atrophy of the hippocampus).
- Parkinson's disease: transverse SWI (to detect abnormalities in the red nucleus and substantia nigra).

(4) MRI sequences for brain structure and function research:
- 3D-T1WI structural imaging (for accurate anatomical segmentation and registration of functional brain imaging).
- DTI (to evaluate occult white matter changes and abnormalities in white matter tracts).
- BOLD-fMRI (task-related and resting states, to study the link between brain activation and brain function).

Suggested Readings

Antoch G, Bockisch A. Combined PET/MRI: a new dimension in whole-body oncology imaging? Eur J Nucl Med Mol Imaging. 2009;36(Suppl 1): S113–20.

Bogner W, Hangel G, Esmaeili M, et al. 1D-spectral editing and 2D multispectral in vivo(1)H-MRS and (1) H-MRSI-methods and applications. Anal Biochem. 2017;529:48–64.

Boss A, Bisdas S, Kolb A, et al. Hybrid PET/MRI of intracranial masses: initial experiences and comparison to PET/CT. J Nucl Med. 2010;51(8):1198–205.

Castillo M. History and evolution of brain tumor imaging: insights through radiology. Radiology. 2014;273(2 Suppl):S111–25.

Cattaneo PW, De Gerone M, Gatti F, et al. Development of high precision timing counter based on plastic scintillator with SiPM readout. IEEE Trans Nucl Sci. 2014;61(5):2657–66.

Delso G, Kemp B, Kaushik S, et al. Improving PET/MR brain quantitation with template-enhanced ZTE. Neuroimage. 2018;181:403–13.

Freitag MT, Fenchel M, Bäumer P, et al. Simultaneous carotid PET/MR: feasibility and improvement of magnetic resonance-based attenuation correction. Int J Cardiovasc Imaging. 2016;32(1):61–71.

Hammer BE. NMR-PET scanner apparatus. 1990, WO9101503A1.

Herzog H, Pietrzyk U, Shah NJ, et al. The current state, challenges and perspectives of MR-PET. Neuroimage. 2010;49(3):2072–82.

Judenhofer MS, Wehrl HF, Newport DF, et al. Simultaneous PET-MRI: a new approach for functional and morphological imaging. Nat Med. 2008;14(4):459–65.

Liu F, Jang H, Kijowski R, et al. Deep learning MR Imaging-based attenuation correction for PET/MR imaging. Radiology. 2018;286(2):676–84.

Martinez-Möller A, Nekolla SG. Attenuation correction for PET/MR: problems, novel approaches and practical solutions. Z Med Phys. 2012;22(4):299–310.

Mehranian A, Zaidi H. Joint estimation of activity and attenuation in TOF-PET/MR using constrained Gaussian mixture models. IEEE Trans Med Imaging. 2015;34(9):1808–21.

Merlo Pich E, Jeromin A, Frisoni GB, et al. Imaging as a biomarker in drug discovery for Alzheimer's disease: is MRI a suitable technology? Alzheimers Res Ther. 2014;6(4):51–8.

Miller-Thomas MM, Benzinger TL. Neurologic applications of PET/MR imaging. Magn Reson Imaging Clin N Am. 2017;25(2):297–313.

Okazawa H, Tsujikawa T, Higashino Y, et al. No significant difference found in PET/MRI CBF values reconstructed with CT-atlas-based and ZTE MR attenuation correction. EJNMMI Res. 2019;9(1):26.

Páez D, Orellana P, Gutiérrez C, et al. Current status of nuclear medicine practice in Latin America and the Caribbean. J Nucl Med. 2015;56(10):1629–34.

Pichler BJ, Wehrl HF, Kolb A, et al. Positron emission tomography/magnetic resonance imaging: the next generation of multimodality imaging? Semin Nucl Med. 2008;38(3):199–208.

Roncali E, Cherry SR. Application of silicon photomultipliers to positron emission tomography. Ann Biomed Eng. 2011;39(4):1358–77.

Saeed U, Compagnone J, Aviv RI, et al. Imaging biomarkers in Parkinson's disease and Parkinsonian syndromes: current and emerging concepts. Transl Neurodegener. 2017;6:8.

Sailer AMH, Grutters JP, Wildberger JE, et al. Cost-effectiveness of CTA, MRA and DSA in patients with non-traumatic subarachnoid haemorrhage. Insights Imaging. 2013;4(4):499–507.

Shao Y, Cherry SR, Farahani K, et al. Simultaneous PET and MR imaging. Phys Med Biol. 1997;42(10):1965–70.

Willekens I, Lahoutte T, Buls N, et al. Time-course of contrast enhancement in spleen and liver with Exia 160, Fenestra LC, and VC. Mol Imaging Biol. 2009;11(2):128–35.

Xi D, Xie Q, Zhu J, et al. Optimization of the SiPM pixel size for a monolithic PET detector. Phys Procedia. 2012;37:1497–503.

Yamamoto S, Watabe T, Watabe H, et al. Simultaneous imaging using Si-PM-based PET and MRI for development of an integrated PET/MRI system. Phys Med Biol. 2012;57(2):N1–13.

2 Research Applications of PET Imaging in Neuroscience

Jiehui Jiang

With the recent advances in nuclear medicine imaging equipment and the development of new imaging agents, the applications of positron emission tomography (PET) imaging in the field of neuroscience have grown rapidly. PET imaging allows for the visualization of physiological and pathological changes in the living brain at a molecular level, providing vital and valuable information for the diagnosis and treatment of central nervous system (CNS) diseases. This chapter primarily focuses on the principles of PET imaging, the processing of PET data, and the research applications of PET in neuroscience.

2.1 Principles of PET Imaging

2.1.1 Physical Principles of PET Imaging

PET imaging involves the detection of a radiotracer labelled with a positron-emitting nuclide within the body. When the radionuclide-containing tracer is injected into the body, the radionuclide bound to the tracer accumulates in the target organ(s), from which it emits positrons. Each positron travels approximately 1–3 mm and then collides with a random body tissue. This collision generates annihilation radiation, producing a pair of 511 keV gamma (γ) photons that travel 180° relative to each other. By placing a pair of detectors in the direction of flight for the photon pair, the two photons can be captured simultaneously. The line connecting the two detectors receiving the photon pair is known as the line of response (LOR) and implies that the annihilation event must lie somewhere along this straight line. Therefore, by arranging multiple sets of detectors in a 360° ring, we can obtain one-dimensional information about the lines connecting multiple detector pairs. These signals are then subjected to back-projection and mathematical processing, to obtain a tomographic image of the distribution of the radiotracer.

The positron-emitting radionuclides involved in the process of the generation of annihilation radiation are generally proton-rich nuclides that emit positrons when they decay. The proton in the nucleus decays into a neutron, while also releasing a positron and a neutrino, as shown in Eq. (2.1):

$$P \rightarrow n + \beta^{+} + \upsilon \tag{2.1}$$

where P is the proton, n is a neutron, β^{+} is a positron, and υ is a neutrino. A positron has the same mass as an electron, and the same magnitude of electric charge like an electron, but positive rather than negative. Positron emission (or β^{+} decay) generally occurs in artificial radionuclides.

J. Jiang (✉)
Institute of Biomedical Engineering,
School of Life Sciences, Shanghai University,
Shanghai, China
e-mail: jiangjiehui@shu.edu.cn

J. Lu, G. Zhao (eds.), *PET/MR: Functional and Molecular Imaging of Neurological Diseases and Neurosciences*, https://doi.org/10.1007/978-981-19-9902-4_2

Table 2.1 Physical properties of commonly used positron-emitting radionuclides

Radionuclide	Half-life (min)	Maximum positron energy (MeV)	Maximum range (mm)	Average range (mm)
^{11}C	20.3	0.96	5.0	0.28
^{13}N	10.0	1.19	5.4	0.60
^{15}O	2.0	1.70	8.2	1.10
^{18}F	109.8	0.64	2.4	0.22
^{68}Ga	67.8	1.89	9.1	1.35
^{82}Rb	1.3	3.35	15.6	2.60

The preparation of PET radiotracers requires the generation of radioisotopes by bombarding a target with a proton beam in a cyclotron. Currently, the most commonly used PET radionuclide is ^{18}F, which has a half-life of approximately 110 min. In comparison, other PET radionuclides (^{11}C, ^{13}N, and ^{15}O) have shorter half-lives (20, 10, and 2 min, respectively). Radionuclides commonly used in neuroimaging include ^{11}C, ^{18}F, and ^{15}O.

The physical properties of commonly used positron-emitting radionuclides are shown in Table 2.1.

2.1.2 PET Scanning System

The primary function of the PET scanner, which is composed of the gantry, examination table, electronic cabinet, operator console, analysis workstation, and printing equipment, is to record the annihilation events.

2.1.2.1 Gantry

The gantry is the largest component of the PET scanner and primarily consists of the detector ring, rod source, radiation shielding equipment, event detection system, and coincidence circuitry.

Detector

The detector is the most crucial component of the PET imaging process. It serves to capture incident γ photons and absorb their energy, from which it generates electrical signals that can then be processed by subsequent circuits. The recorded electrical signals provide information for processing, such as the energy deposited in the detectors by the γ photons and the time and position of photon interactions with the scintillation crystals. The PET detector is composed of scintillation crystals, photomultiplier tubes (PMTs), and related electronic circuits. Of these components, the scintillation crystals and PMTs are the core components of the detector, and their arrangement determines its structure. The performance of the PET scanner is dependent on the detector, which plays a decisive role in the scanner's core performance indicators, including spatial resolution, temporal resolution, and sensitivity.

PET detectors are generally constructed using high-density crystals such as bismuth germanium oxide (BGO), lutetium oxyorthosilicate (LSO), or lutetium yttrium oxyorthosilicate (LYSO), which are segmented into smaller elements. Thus, one detector block consists of one crystal block and its coupled PMTs. The most classic arrangement is the 4 × 64 array, in which each detector block is composed of 4 PMTs coupled to 64 crystal elements. Multiple detector blocks are tightly arranged to form a ring, and multiple detector rings are arranged to form a cylinder. The X-Y plane is the PET cross-section, which is parallel to the plane of the detection ring. The Z axis is the long PET axis, which is perpendicular to the plane of the detection ring.

The detectors used in PET scanners can be classified into two major types according to the crystals used: scintillation detectors and semiconductor detectors. Scintillation detectors are the more widely used detectors in PET imaging systems. Nevertheless, semiconductor detectors have gradually been utilized in PET scanners used for small animals, due to their excellent energy resolution and direct photoelectric conversion during detection.

Scintillation Detectors

Scintillation detectors are detectors that use the flash of light (i.e., scintillation) produced when

radiation interacts with certain substances to detect ionizing radiation. They are primarily composed of the scintillator, light guide, and PMTs.

1. Scintillator

The scintillator is the core component of the scintillation detector, and its properties have a direct impact on the performance of the detector, particularly its energy, time, and position localization. The scintillator used in early PET systems was thallium-doped sodium iodide (NaI[Tl]). NaI(Tl) has a high light yield and good spatial resolution, but also has poor stopping power and longer luminescence decay, and is prone to deliquescence. As the crystal manufacturing technology advanced, new scintillation crystals were gradually introduced. BGO crystals have a large decay constant, low light yield, and poor energy resolution, but have a high density, strong stopping power, and high sensitivity, and can be used for two-dimensional (2D) PET imaging. LSO and LYSO crystals are currently the preferred choices for scintillators in PET scanners due to their fast response, high light yield, and high density.

Newer halide scintillators, such as cerium-doped lanthanum bromide ($LaBr_3$:Ce), cerium bromide ($CeBr_3$), and cerium-doped lutetium iodide (LuI_3:Ce), have a number of excellent properties, including high light yield, rapid decay, and high energy density. Unfortunately, the raw materials for these halide crystals are costly and difficult to prepare, which has hindered their widespread application in PET imaging. Additionally, cerium-doped gadolinium aluminum gallium garnet ($Gd_3[Al,Ga]_5O_{12}$:Ce, GAGG:Ce), used in a multicomponent garnet scintillator, has excellent light yield, good energy resolution, and no issues with deliquescence or self-radioactivity, exhibiting exceptional comprehensive performance compared to other scintillation crystals. Table 2.2 lists the scintillation crystals most frequently used in PET imaging systems, along with their technical performance indicators.

2. Light guide

Light guides are primarily made of silicone oil or organic glass and are used to fill the gaps between the crystal scintillator and the PMTs. Light guides are meant to minimize the total internal reflection of photons interacting with air, and enhancing the efficiency of the photons entering the PMTs.

3. Photomultiplier tube (PMT)

PMTs are vacuum electron-tube devices that convert weak light signals, those at wavelengths of 200–1200 nm, into electrical signals.

Semiconductor Detectors

Semiconductor detectors use semiconductive materials as the detection medium and work by converting radiant energy into electrical signals. Compared to traditional scintillation detectors, semiconductor detectors bypass the need for multiple energy conversions and have a low signal noise, high energy resolution, and compact device structure. Semiconductor detectors detect radiation based on the generation of electron–hole pairs within the crystals. An electric field is

Table 2.2 Technical performance indicators of common scintillation crystals

Scintillator	Density (g/cm^3)	Light yield (photons/MeV)	Decay time (ns)	Wavelength of luminescence center (nm)	Energy resolution (%)
NaI:T1	3.7	41,000	230	415	9.0 (140 keV)
CsI:T1	4.5	66,000	800	550	14.0 (140 keV)
BGO	7.1	9000	300	480	12.0 (511 keV)
LSO:Ce	7.4	30,000	40	420	9.1 (511 keV)
LYSO:Ce	7.1	32,000	45	420	7.1 (511 keV)
$LaBr_3$	5.3	63,000	16	358	3.3 (511 keV)
LuAP	8.3	10,000	18	365	11.4 (511 keV)
GSO	6.7	12,500	60	440	7.9 (511 keV)
GAGG:Ce	6.6	56,000	90	520	4.9 (662 keV)

applied at both ends of the detector, which causes the electrons and electron holes to drift toward the anode and cathode, respectively. This results in the formation of an output charge, which converts radiation into electrical signals, thus detecting the radiation emitted.

Early semiconductor detectors were primarily composed of silicon (Si) and germanium (Ge). However, both Si and Ge have a relatively narrow band gap, meaning that early detectors needed to operate at liquid nitrogen temperatures in order to suppress the thermal noise produced by the detectors themselves. Furthermore, Si and Ge have lower effective atomic numbers; therefore, their detection efficiencies are too low for detecting γ- or X-rays. In recent years, compound semiconductors, such as cadmium telluride (CdTe) and cadmium zinc telluride (CZT), have been created and utilized in semiconductor detectors. Compared to Si- and Ge-based semiconductor detectors, CdTe- and CZT-based detectors have wider band gaps, allowing them to operate at room temperature. Moreover, they have higher energies and spatial resolutions and can be used to construct detection modules of smaller sizes. Therefore, semiconductor detectors have been regarded as viable alternatives to scintillation detectors.

1. Rod source

A rod source uniformly encapsulates germanium-68 (^{68}Ge) or cesium-137 (^{137}Cs) within a small hollow rod. Depending on the equipment, there are usually 1–3 rod sources with different activities for transmission scans, blank scans, and quality control.

2. Shielding

The internal shielding of the PET scanner consists of two parts: (1) Thick lead plates (or septa) on both sides of the entire detector ring, which serve to shield the detection rays; and (2) 1 mm thick, ring-shaped tungsten plates interposed between individual detector rings, which serve to shield incident photon pairs from the field of view (FOV) of other rings, similar to the function of a collimator.

3. Detection system and coincidence circuitry

The role of an event detection system is to collect incoming electrical signals from the detector, determine if they are valid (511 keV) γ photon signals and transmit information about the position of any valid γ photon signals. The coincidence circuitry receives the photon event signal from the coincidence detection system. Each detector that registers a γ photon generates a timed pulse, which is fed into the coincidence circuitry to identify and select true coincidence events.

Under normal circumstances, a very small window ($\leq$ 15 ns) is set for the coincidence circuits. Timed pulses that are registered simultaneously within this time window are regarded as γ photon pairs generated by the same positron annihilation event and are subsequently recorded by the coincidence circuitry. Based on the positional and temporal information gathered, it is possible to reconstruct a three-dimensional (3D) PET image. Furthermore, annihilation γ photon pairs can only be detected within the FOV of two opposing detectors (180° apart). The technique of using the coincidence between the output pulses from two opposing detectors to determine the position of a scintillation event is known as electronic collimation, which is a major feature of PET imaging. It forgoes the need for heavy lead collimators, improves the sensitivity and uniformity of the point-source response function, avoids the negative effects of lead collimators on resolution and uniformity, and greatly improves detection sensitivity.

Although the coincidence circuitry can detect simultaneous scintillation events, in reality, there is always a time difference between the triggering of the two detectors. This time difference is known as the resolution time and implies that γ photons which arise from different positions but are incident on two opposing detectors within the resolution time are also recorded. Coincidence events which are not generated by annihilation radiation are known as random coincidences. Additionally, γ photons may also randomly undergo Compton scattering during flight, which changes the course of the photons and results in a different LOR to that of the original event. This is known as scattered coincidence.

Random and scattered coincidences create image noise, reducing image resolution and contrast, thereby affecting image quality. Increasing the coincidence count rate to a certain level will lead to a quadratic increase in the count rates for random and scattered coincidences, whereas increasing the degree of activity to a certain extent will, instead, result in poorer image quality. Therefore, we cannot improve the image quality of PET scans simply by increasing radiotracer activity alone.

4. Examination table

The examination table holds the patient during the PET scan. It moves the patient to position the part of the body to be examined within the FOV of the scanner, depending on the requirements of the examination.

5. Electronic cabinet

The electronic cabinet primarily contains the central processing unit, input and output systems, internal and external storage systems, and other components. Its main function is to perform image reconstruction, as well as the processing and storage of image data.

6. Image analysis workstation

The workstation is primarily composed of a computer system with PET-specific software. Its functions include image reconstruction and display, data storage, and data transmission.

7. Printing equipment

The printing equipment consists of image output systems, such as printers and laser cameras. Its main function is to output images, text, or other materials.

2.1.3 PET Image Acquisition

PET image acquisition can be categorized into two types: emission scanning and transmission scanning. Emission scanning can further be divided into the following categories: 2D, 3D, static, dynamic, gated, local, and whole-body acquisition.

2.1.3.1 Emission Scanning

When positron-emitting nuclides enter the human body and decay, they each emit one positron, which travels a very short distance, 1–3 mm, through the nearby body tissue. Once its kinetic energy disappears, the positron collides with an electron to generate annihilation radiation, thus creating two γ photons (both with an energy of 511 keV) that travel in opposite directions. The process by which the PET scanner collects information about these photon pairs to determine the location and quantity of the radiotracer is known as emission scanning.

2D and 3D Acquisition

A 2D acquisition involves the placement of shields (known as septa) between the individual detector rings. During 2D acquisition, the septa block photons from interacting with other detector rings and allow the detection of photon pair signals only within the same ring. Three-dimensional acquisition is a rapid mode in which the septa are removed, and the detectors can detect photon pair signals from other detector rings, expanding the detection range to the entire axial FOV. The intensity of photon pair signals detected in 3D acquisition is 8–12 times higher than that of 2D acquisition, which also significantly enhances sensitivity. However, this also implies that there is a marked increase in scattered and random coincidences in 3D acquisition, leading to a low signal-to-noise ratio and necessitating scatter and random coincidence correction. Three-dimensional acquisition is currently widely used in clinical practice. The schematic diagrams for 2D and 3D acquisition are shown in Fig. 2.1.

Static and Dynamic Acquisition

Static acquisition is the most commonly utilized mode of PET imaging. It involves waiting for a fixed amount of time after the imaging agent is injected into the patient and acquiring the images when the agent has reached equilibrium. Dynamic acquisition refers to a continuous, dynamic mode

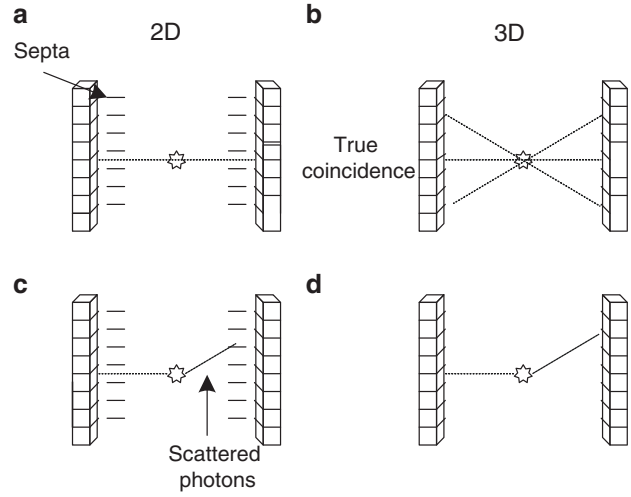

Fig. 2.1 Schematic diagrams of 2D and 3D PET acquisition

of data collection which is performed while actively injecting the imaging agent to obtain a continuous, dynamic image sequence. This enables us to observe the spatial changes of the imaging agent in the body, and to study dynamic changes in vivo.

Gated Acquisition

Gated acquisition includes cardiac and respiratory gated acquisition. As cardiac and respiratory movements are characterized by their cyclic nature, gating can be used to collect information that is synchronized with these cycles, in order to eliminate the effects of cardiac and respiratory motion.

Local and Whole-Body Acquisition

Local acquisition is primarily utilized for the imaging of specific organs (e.g., brain, heart) or certain parts of the body, while whole-body acquisition is mainly used for the diagnosis and evaluation of malignant tumors and associated metastases.

2.1.3.2 Transmission Scanning

Transmission scanning refers to the process in which a rod source is rotated around the body to collect the leftover radiation after the external radioactive source has exited the human body. By combining the results of the transmission and blank scans, we can calculate the attenuation coefficient of the tissues. Hence, transmission scanning can be used to perform attenuation correction on the data from the emission scan.

2.1.4 PET Image Reconstruction

The raw data used in the process of PET image reconstruction includes the one-dimensional projections of the radiation emitted from the patient (i.e., a set of parallel line integrals or ray sums). To convert these data into a usable form, they must first be mathematically transformed (or reformatted) and reconstructed into a set of horizontal images. The primary methods of image reconstruction are analytical, iterative, and deep learning.

2.1.4.1 Analytical Methods

Analytical methods are back-projection methods based on the central slice theorem, with filtered back-projection (FBP) being the most commonly used method. Once the acquisition of PET data is complete, it is confirmed that count values along the LORs between the detectors are directly proportional to the integrals of the radioactivity along these LORs. These line integrals are known as projections, and based on these projection data, we can perform the image reconstruction for each tomographic plane.

In FBP reconstruction, the projection data are convolved under a given projection angle using a

filter to obtain the corrected projection data, followed by the back-projection (i.e., reverse to the projection direction) of the corrected projection data to reconstruct the image. In order to improve the computational speed, FBP always converts the raw projection data to the frequency domain for processing. In the frequency domain, the convolution operation is a simple multiplication, which substantially improves the speed of reconstruction. Fourier transform is always applied in FBP processing to convert the image from the spatial to the frequency domain. Once the reconstruction is complete, the inverse Fourier transform is applied to convert the image from the frequency to the spatial domain for ease of image interpretation. The FBP technique primarily includes the following steps:

1. Fourier transform: raw data are converted into frequency domain functions using the Fourier transform
2. Filter: pre-filtering is performed using the ramp filter function
3. Back-projection operation: the image is reconstructed using the back-projection technique
4. Second filter: the appropriate filter function and parameters are selected to filter the reconstructed image and eliminate the high-frequency noise of star artifacts and
5. Inverse Fourier transform: the image is converted from the frequency to the spatial domain for ease of display and interpretation.

2.1.4.2 Iterative Methods

Iterative reconstruction is an algorithm-based method of image processing characterized by convergence. It primarily involves the performance of multiple rounds of iterative algorithm-based comparisons in order to ensure the consistency of the reconstructed data with the actual image data, and is therefore much more computationally expensive. As the computing speeds of microcomputers continue to increase, the application of this reconstruction technique has grown in popularity. The principle behind iterative reconstruction is very simple: at the start of reconstruction, a set of initial cross-sectional estimates is arbitrarily assigned, which is usually a data matrix with all elements set to 1 and using the same size as the original acquisition matrix. Based on these initial estimates, the simulated projection data is calculated and compared to the original projection data, in order to determine the amount of correction needed for each pixel. Using this corrective data, adjustments are made to the matrix values of the initial image data. The adjusted image is then repeatedly subjected to the steps above, and multiple rounds of iterations are performed until a predetermined level of accuracy is attained. A flowchart summarizing iterative reconstruction is shown in Fig. 2.2.

The greatest advantage of iterative reconstruction is the ability to introduce various physical factors and statistical models during the reconstruction process, in order to achieve high-resolution images. One of the more widely used methods is the statistical iterative method, which

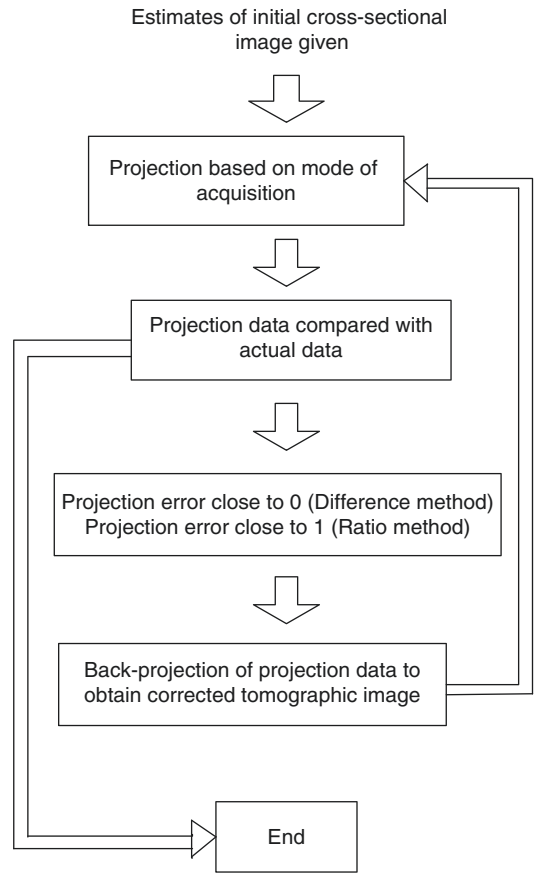

Fig. 2.2 Flowchart of iterative tomographic image reconstruction